ChemComm

Accepted Manuscript

ROYAL SOCIETY OF CHEMISTRY

rsc.li/chemcomm

View Article Online
DOI: 10.1039/C9CC00113A

Journal Name

COMMUNICATION

A lysosome-targetable dual-functional fluorescent probe for imaging intracellular viscosity and beta-amyloid

Hui-ya Tan,[a] Yu-tai Qiu,[a] Han Sun, [a] Jin-wu Yan, [*a,b,c] and Lei Zhang [*a,b,c]

Received 00th January 20xx,
Accepted 00th January 20xx

DOI: 10.1039/x0xx00000x

www.rsc.org/

A lysosome-targetable dual-functional fluorescent probe was rationally designed and developed for imaging intracellular lysosomal viscosity and beta-amyloid. More importantly, the real-time tracking of dynamic movement of lysosome, as vesicle structure, has been achieved by using Lyso-MC.

Alzheimer's disease (AD), an age-related pathology, leads to progressive cognitive decline, communication barrier, language disorder and loss of self-care ability.[1-3] Besides, AD has affected millions of people worldwide with 5 million new cases every year,[4] however, the symptomatic treatment only mildly improves the symptoms of AD but still incurable due to the unclear pathophysiological mechanism of AD.[5,6] The toxic amyloid-β peptide (Aβ) generates from APP (Amyloid Precursor Protein) after the sequential action of β- and γ-secretase and accumulates constantly to the senile plaques, the hallmark of AD, which are considered to be basic pathological targets for primary prevention, early diagnosis and treatment of the disease.[5,6] It has been pointed out that intracellular Aβ is involved in the early stage of AD and spreads from neuron to neuron, directly causing neurotoxicity and triggering AD pathology.[7-9] Several studies have found that amyloid precursor protein (APP) and amyloid-β peptide (Aβ) are generated from autophagy and endocytic pathway,[10-13] besides, AD is characterized by lysosomal dysfunction and a massive accumulation of lysosomal-related vesicles in the degenerating neurons.[11,14,15] Moreover, increasing studies point out that the dysfunction of autophagy pathway would be conducive to Aβ accumulation in pathological conditions.[11] Besides, much evidence advocates that the lysosomal system, an acidic vesicular compartment containing various hydrolases, is related to Aβ production and neurotoxicity.[16,17] In addition, restoring autophagy or improving lysosomal degradation of intracellular Aβ may be a potential therapeutic approach to treat AD.[10,13] Therefore, monitoring cellular lysosomal movement or physiological changes and intracellular Aβ could provide a better understanding for AD pathology and its early diagnosis.

It is reported that the lysosomal viscosity is an important benchmark for lysosome situation and it reflects the status and function of this organelle,[16,18,19] therefore, tracing lysosome or monitoring its viscosity changes is of great benefit for AD diagnosis and pathological studies. Recently, many Aβ fluorescent probes[20-22] and many lysosome-targetable fluorescent probes imaging viscosity[19,23,24] have been reported. However, as we know, the lysosome-targetable dual-functional fluorescent probe imaging both viscosity and Aβ aggregates at cellular level has not been reported.

Herein, a fluorescent probe (**Lyso-MC**) for sensitively imaging intracellular lysosome and Aβ aggregates was reasonably designed and developed. The neutral merocyanine dye (**MC-1**)[25] was selected as the fluorophore to design this probe, which was reported previously by our group as a good scaffold imaging Aβ plaques *in vivo* and imaging viscosity at cellular level reported by Lin's group.[26] However, the low quantum yield and photo-stability of **MC-1** restricted its further application. In this study, 3-morpholinopropylamine moiety was rationally introduced as electron-donor to enhance the conjugation of π electron so as

[a] School of Biology and Biological Engineering, South China University of Technology, Guangzhou 510006, P.R. China.
[b] Guangdong Provincial Engineering and Technology Research Center of Biopharmaceuticals, South China University of Technology, Guangzhou 510006, P.R. China.
[c] Joint International Research Laboratory of Synthetic Biology and Medicine, South China University of Technology, Guangzhou 510006, P.R. China. E-mail: yjw@scut.edu.cn; lzhangce@scut.edu.cn.

Electronic Supplementary Information (ESI) available: Synthesis and characterization of probe, experimental procedures, and supplemental spectra and graphs. See DOI: 10.1039/x0xx00000x

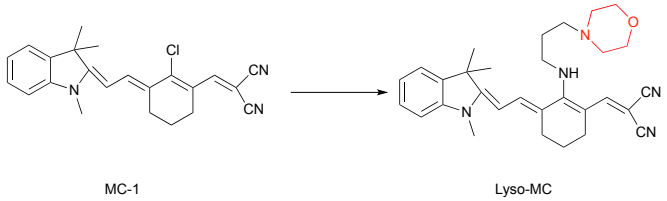

MC-1 Lyso-MC

Scheme 1 Chemical structures of **MC-1** and **Lyso-MC**.

View Article Online
DOI: 10.1039/C9CC00137A

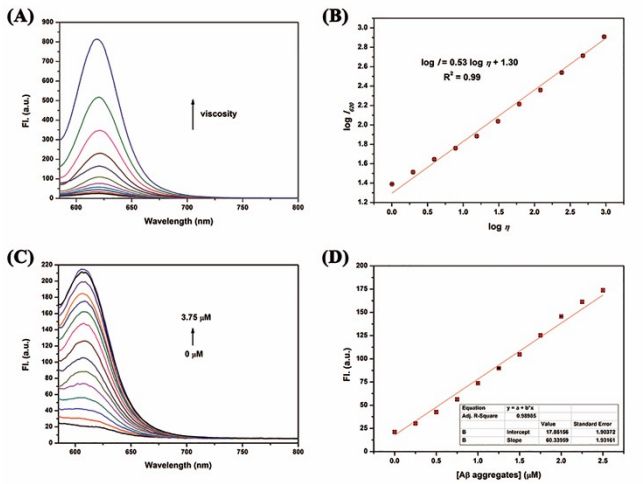

Fig. 1 (A) Solvent viscosity-dependent fluorescence changes of **Lyso-MC** (0.25 μM) in water-glycerol system; (B) The linear relationship between log I_{620} and log η of **Lyso-MC**; (C) Fluorescence spectroscopic titration of **Lyso-MC** (0.25 μM) towards $A\beta_{1\text{-}42}$ aggregates in PBS buffer (pH=7.4) ; (D) Emission intensity of **Lyso-MC** as a function of the concentration of $A\beta_{1\text{-}42}$ aggregates in PBS buffer (pH=7.4).

to improve the fluorescence quantum yield, and functioned as lysosomal targeting group[19,23,24]. As we know, **Lyso-MC** was the first lysosome-targetable dual-functional probe monitoring viscosity and Aβ aggregates at cellular level.

The synthesis of **Lyso-MC** is outlined in Scheme S1 (ESI†) and its structure (Scheme 1) was confirmed by ^{1}H and ^{13}C NMR spectroscopy and HR-MS. The fluorescence response spectra of **Lyso-MC** were first investigated in a water-glycerol system with increasing viscosity. As shown in Fig. 1A, **Lyso-MC** emitted at 615 nm along with the weakest fluorescence in an absolute water medium. Meanwhile, the emission intensity showed a dramatic fluorescence enhancement (33-fold, Table S1, ESI†) and the emission wavelength red-shifted to 620 nm due to the viscous increasement which was caused by the increasing ratio of glycerol in water-glycerol system. In addition, as shown in Fig. 1B, the good linear relationship between log I_{620} and log η (R^2 = 0.99, x = 0.53) was quantitatively gained according to the Förster-Hoffmann equation. Moreover, as shown in the Fig. S2 (ESI†), the polarity environment only had an influence on the emission wavelength where **Lyso-MC** showed higher absorption and emission wavelengths when increasing the polarity of the surrounding environment. Compared with the strong fluorescence of **Lyso-MC** in glycerol, its fluorescence in other solvents with different polarities was negligible (Fig. S3, ESI†), therefore, its fluorescence intensity was insensitive to polarity changes. In the pH titration experiment, **Lyso-MC** could not be disturbed by the lysosomal pH range (pH = 4.5~5.0) and only affected by viscosity (Fig. S4, ESI†). Besides, **Lyso-MC** was not interfered by various amino acids and ions (Fig. S5, ESI†), exhibiting good selectivity towards viscosity. These results indicated that the **Lyso-MC** was a stable viscosity fluorescent probe for detecting viscosity in lysosomes.

We further investigated the fluorescence response of **Lyso-MC** towards the synthetic $A\beta_{1\text{-}42}$ aggregates, Aβ monomer, BSA and HSA. As expected, the probe exhibited a remarkable (10-fold) fluorescence intensity in the presence of $A\beta_{1\text{-}42}$ aggregates at a low final concentration of 0.25 μM. As displayed in Fig. S5(ESI†), less fluorescence responses were observed upon interaction with BSA, HSA and Aβ monomer, indicating low nonspecific binding and its good selectivity towards $A\beta_{1\text{-}42}$ aggregates. Next, the interaction between **Lyso-MC** and $A\beta_{1\text{-}42}$ aggregates were further studied by the fluorescence titrations. As shown in the Fig. 1C, upon titration with $A\beta_{1\text{-}42}$ aggregates, the emission wavelength blue-shifted to 610 nm and the emission intensity was significantly enhanced. Besides, it showed a good linear relationship (R^2 = 0.9899) with $A\beta_{1\text{-}42}$ aggregates concentration ranging from 0 to 2.5 μM (Fig. 1D). Moreover, the detection limit of **Lyso-MC** was determined to be as low as 10.2 nM (Table S2, ESI†). After the saturation binding assay between **Lyso-MC** and $A\beta_{1\text{-}42}$ aggregates, the binding constant was calculated to be 31.74 nM, indicating that the probe **Lyso-MC** exhibited moderate affinity towards Aβ aggregates (Table S2, ESI†). In addition, the LogP value was measured to be 2.63, predicting that **Lyso-MC** had its potential in good blood brain barrier (BBB) penetration. Besides, the red and blue shift was observed for **Lyso-MC** in viscous and hydrophobic environments respectively, therefore it could be

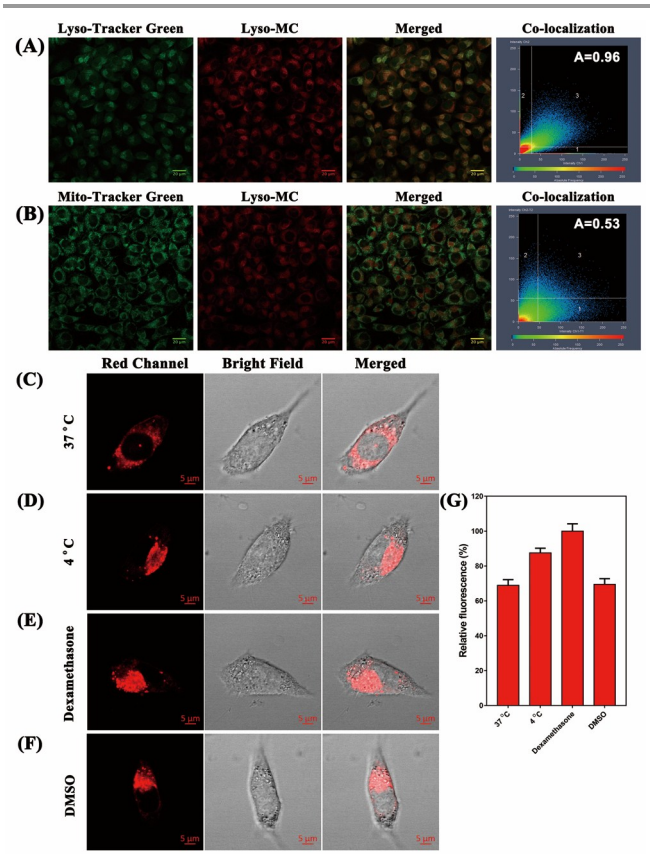

Fig. 2 (A) Colocalization fluorescence images of SH-SY5Y cells co-incubated with **Lyso-MC** (5 μM) and Lyso Tracker Green (1 μM); (B) Colocalization fluorescence images of SH-SY5Y cells co-incubated with **Lyso-MC** (5 μM) and Mito Tracker Green (1 μM). Scale bars: 20 μm; (C) Confocal fluorescence images of SH-SY5Y cells incubated with **Lyso-MC** (5 μM) only at 37 ° C; (D) Confocal fluorescence images of SH-SY5Y cells incubated with **Lyso-MC** (5 μM) only at 4 ° C; (E) Cells were incubated with **Lyso-MC** (5 μM) only at 37 ° C for 30 min following by treatment with dexamethasone (5 μM) for another 10 min; (F) Cells were incubated with **Lyso-MC** (5 μM) only at 37 ° C for 30 min following by treatment with DMSO (10 μL) for another 30 min; (G) Analysis of the relative fluorescence intensity in SH-SY5Y cells treated in different incubation situations (n=3, data were obtained from ImageJ Software), Scale bars: 5 μm.

used as dual-functional fluorescent probe to distinguish viscosity changes and Aβ aggregates on the basis of the different emission wavelengths in the different environments.

Due to its good response to viscosity, we further investigated the application of **Lyso-MC** in living cells. Before fluorescent imaging in living cells, the cytotoxicity of **Lsyo-MC** was first assessed in SH-SY5Y and Hela cells. A standard MTT assay in SH-SY5Y and Hela cells showed that over 80% cells remained alive when 12.5 μM **Lyso-MC** was internalized for 12 h (Fig. S7, ESI†), indicating that the probe exhibited weak cytotoxicity. Then, the fluorescence imaging of **Lyso-MC** in living SH-SY5Y and Hela cells was performed by confocal laser scanning microscopy. The cells exhibited negligible fluorescence in the absence of **Lyso-MC**, while the cells incubated with **Lyso-MC** exhibited strong red fluorescence and the fluorescence intensity was dose and time dependent, indicating that **Lyso-MC** permeated the membrane and can stain living cells (Fig. S8 and Fig. S9, ESI†).

Encouraged by the good membrane-permeable of the probe, we further investigated the co-localization of **Lyso-MC** in lysosomes of SH-SY5Y cells with commercially available Lyso-tracker Green DND-26 and Mito-tracker Green FM. As shown in Fig. 2, **Lyso-MC** overlapped very well with Lyso-Tracker Green with the overlap coefficient as high as 0.96 between **Lyso-MC** and Lyso-Tracker Green, while the coefficient between **Lyso-MC** and Mito-Tracker green was only 0.53. The results indicated that **Lyso-MC** was a lysosome-targetable probe. Meanwhile, we investigated the photo-stability of **Lyso-MC** inside cells, which was of great importance for imaging the viscosity of lysosome. Then the commercially available Lyso-Tracker Green was used as a comparison. The SH-SY5Y cells were exposed to 561 nm channel after incubating with **Lyso-MC** while the Lyso-Tracker Green group was exposed to 488 nm channel. After 10 min continuous illumination, the signal loss for **Lyso-MC** and Lyso-Tracker Green was 72% and 88%, respectively (Fig. S10, ESI†). Therefore, the probe exhibited moderate photo-stability both in solution (Fig. S6, ESI†) and in living cells.

It is known that a lower temperature contributes to the intracellular viscosity increasement and dexamethasone used as a clinic drug has been proved to be effective in increasing lysosomal viscosity.[27,28] With the aim to investigate the ability of **Lyso-MC** to monitor the variation of intracellular lysosomal viscosity, the living SH-SY5Y cells was first incubated with the probe (5 μM) at different temperatures. As shown in Fig. 2, the cells incubated at 4 ° C exhibited stronger red fluorescence in red channel when comparing with cells at 37 ° C due to the greater viscosity value at 4 ° C. As a result, **Lyso-MC** could detect the lysosomal viscosity in living cells. Besides, it was clearly found that the fluorescence intensity increased after treatment with dexamethasone (5 μM), indicating that the lysosomal viscosity value was larger than that at 37 ° C. In addition, there were no obvious fluorescence changes when incubated with DMSO (10 μL) compared with incubated with probe at 37 ° C, which further demonstrated that the probe could monitor the variation of lysosomal viscosity without the interference of polarity fluctuation in living cells.

Due to good lysosome-targetable performance of the probe, we investigated the ability of the probe to trace the lysosomes in real time and observed the subcellular structure of lysosome using CLSM with ultra-high-resolution module. The pictures of SH-SY5Y cells incubated with **Lyso-MC** were taken every 4 seconds by CLSM. As shown in Fig. 3, it demonstrated that dynamic lysosomes in living cells were vesicular structure and five different pseudo-colors were intended to clearly show the movements of lysosome at various time points (0, 20, 40, 60 and 80 s). Merged images at various time points and dynamic video indicated that the movements of lysosome were rather active and **Lyso-MC** could trace intracellular lysosome in real-time.

Considering the specific binding of the probe to $A\beta_{1-42}$ aggregates in solution and important pathological action of intracellular Aβ aggregates, the PC12 cells transfected for the overexpression of Aβ (PC12-EGFP-Aβ cells) and the normal PC12 cells taken as controls were conducted to investigate whether **Lyso-MC** could detect Aβ aggregates at cellular level. As shown in Fig. 11SB (ESI†), granular aggregates were detected with **Lyso-MC** in the cytoplasm, which was consistent with immunofluorescence group (Fig. 11SA, ESI†). Meanwhile, there

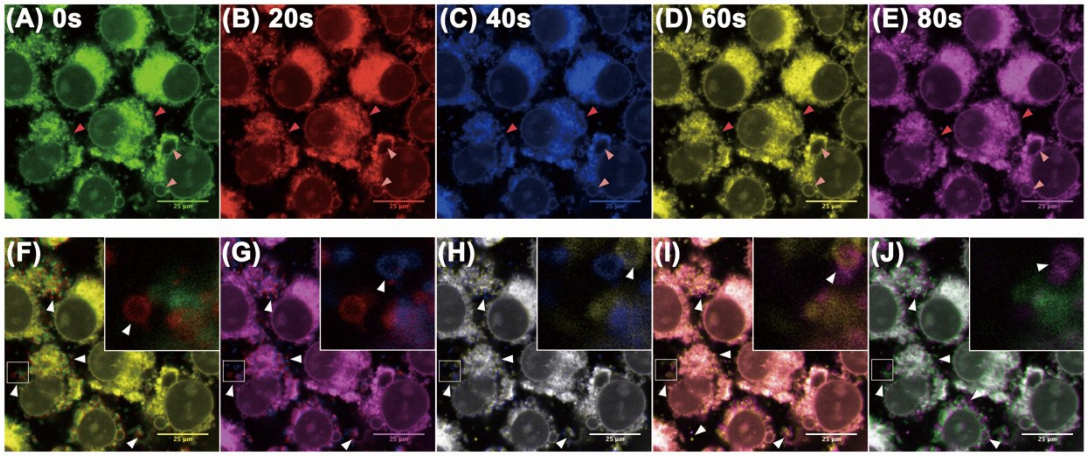

Fig. 3 (A-E) Confocal images of SH-SY5Y cells stained with 5 μM for 30 min. Different pseudo colors were used to illustrate the fluorescence images at 20 s, 40 s, 60 s and 80 s, respectively. (F-J) Merged of images at two different time points: (F) 0 and 20 s, (G) 20 and 40 s, (H) 40 and 60 s, (I) 60 and 80 s, (J) 0 and 80 s. Inset is the zoomed-in image. Dark pink and light pink arrow heads indicate different size of lysosome. White arrow heads indicate the significant movements of lysosome. Scale bars: 25 μm.

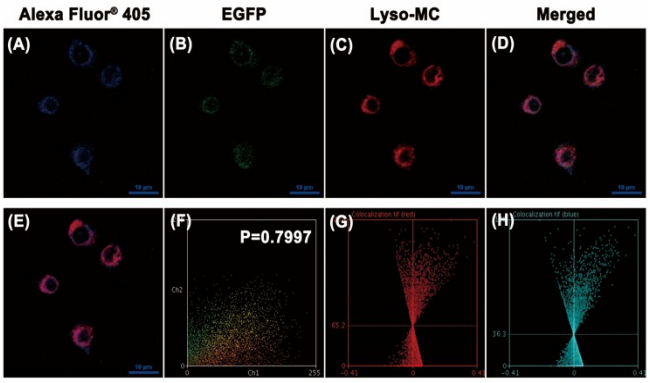

Fig. 4 Co-localization images in transfected PC12 cells after immunofluorescence for $A\beta_{1-42}$ aggregates and then co-stained with **Lyso-MC** (1 μM). (A) Immunofluorescence image from Alexa Fluor®405; (B) Fluorescence image from EGFP; (C) Fluorescence image from **Lyso-MC**; (D) The merged image of (A), (B) and (C); (E) The merged image of (A) and (C); (F) Intensity correlation plot of co-stain **Lyso-MC** and immunofluorescence; ICA plots of (G) stain **Lyso-MC** and (H) stain Alexa Fluor®405 of immunofluorescence. (Analyzed by Image J software)

was negligible fluorescence found in the control PC12 cell (Fig. S12, ESI†). Besides, there was also no fluorescence observed in the PC12-EGFP-Aβ cells with no staining with **Lyso-MC** or immunofluorescence (Fig. S13, ESI†). We also conducted the co-localization experiment for Aβ aggregates in the transfected PC12-EGFP-Aβ cells through co-staining **Lyso-MC** after immunofluorescence assay with secondary antibody Alexa Fluor®405. As shown in Fig. 4, the **Lyso-MC** and Alexa Fluor®405 merged well with a good Pearson's coefficient of 0.7997. The ICA (intensity correlation analysis, which was used to evaluate the intensity distribution of the two co-existing stains) plots for the **Lyso-MC** and Alexa Fluor®405 created an unsymmetrical hourglass-shaped scatterplot which tended to toward positive values (Fig. 4G,H). No matter the ex situ monitor or co-localized for Aβ aggregates, the probe **Lyso-MC** was confirmed to detect Aβ aggregates at cellular level.

In conclusion, a red-emitting dual-functional fluorescent probe with low cytotoxicity based on a neutral merocyanine dye (**MC-1**) was rationally designed and developed for imaging intracellular lysosomal viscosity and Aβ aggregates. The spectral results showed that **Lyso-MC** exhibited an excellent linear relationship between the logarithm of fluorescence intensity and the logarithm of viscosity (R^2 = 0.99, x=0.53), meanwhile, it showed significant turn-on fluorescence response when bound to Aβ aggregates and high sensitivity towards Aβ aggregates (detection limit, 10.2 nM). Besides, **Lyso-MC** has been applied to monitor lysosomal viscosity changes and detect intracellular Aβ aggregates. More importantly, the real-time tracking of dynamic movement of lysosome, as vesicle structure, has been achieved by using **Lyso-MC**. Taking advantage of its remarkable properties, the versatile probe could be a promising imaging tool in the Alzheimer's disease pathology related field.

This work was financially supported by the Natural Science Foundation of Guangdong Province, China (2016A030310463 and 2016A010121004), the National Natural Science Foundation of China (21502056) and the Medical Scientific Research Foundation of Guangdong Province, China (A2018080)。

Conflicts of interest

View Article Online
DOI: 10.1039/C9CC00113A

There are no conflicts to declare.

Notes and references

1 X. Zhang, Y. Tian, C. Zhang, X. Tian, A. W. Ross, R. D. Moir, H. Sun, R. E. Tanzi, A. Moore and C. Ran, *Proc. Natl. Acad. Sci. U. S. A.*, 2015, **112**, 9734-9739.
2 C. Ballard, S. Gauthier, A. Corbett, C. Brayne, D. Aarsland and E. Jones, *The Lancet*, 2011, **377**, 1019-1031.
3 M. Staderini, M. A. Martin, M. L. Bolognesi and J. C. Menendez, *Chem. Soc. Rev.*, 2015, **44**, 1807-1819.
4 H. Tong, K. Lou and W. Wang, *Acta Pharm. Sin. B*, 2015, **5**, 25-33.
5 F. Mangialasche, A. Solomon, B. Winblad, P. Mecocci and M. Kivipelto, *Lancet Neurol.*, 2010, **9**, 702-716.
6 S. Gauthier, L. Wu, P. Rosa-Neto and J. Jia, *Transl. Neurodegener.*, 2012, **1**, 1-13.
7 J. Naslund, V. Haroutunian, R. Mohs, K. L. Davis, P. Davies, P. Greengard and J. D. Buxbaum, *JAMA*, 2000, **283**, 1571-1577.
8 M. Koistinaho, M. Ort, J. M. Cimadevilla, R. Vondrous, B. Cordell, J. Koistinaho, J. Bures and L. S. Higgins, *Proc. Natl. Acad. Sci. U. S. A.*, 2001, **98**, 14675-14680.
9 S. Nath, L. Agholme, F. R. Kurudenkandy, B. Granseth, J. Marcusson and M. Hallbeck, *J. Neurosci.*, 2012, **32**, 8767-8777.
10 R. A. Nixon and A. M. Cataldo, *J Alzheimers Dis.*, 2006, **9**, 277-289.
11 R. A. Nixon, *J Cell Sci.*, 2007, **120**, 4081-4091.
12 R. A. Nixon, D.-S. Yang and J.-H. Lee, *Autophagy*, 2008, **4**, 590-599.
13 F. Pickford, E. Masliah, M. Britschgi, K. Lucin, R. Narasimhan, P. A. Jaeger, S. Small, B. Spencer, E. Rockenstein, B. Levine and T. Wyss-Coray, *J. Clin. Invest.*, 2008, **118**, 2190-2199.
14 K. Inoue, J. Rispoli, H. Kaphzan, E. Klann, E. I. Chen, J. Kim, M. Komatsu and A. Abeliovich, *Mol. Neurodegener.*, 2012, **7**, 48.
15 J.-H. Lee, W. H. Yu, A. Kumar, S. Lee, P. S. Mohan, C. M. Peterhoff, D. M. Wolfe, M. Martinez-Vicente, A. C. Massey, G. Sovak, Y. Uchiyama, D. Westaway, A. M. Cuervo and R. A. Nixon, *Cell*, 2010, **141**, 1146-1158.
16 R. A. Nixon, A. M. Cataldo and P. M. Mathews, *Neurochem. Res.*, 2000, **25**, 1161-1172.
17 J. Han and K. Burgess, *Chem. Rev.*, 2010, **110**, 2709-2728.
18 T. Liu, X. Liu, D. R. Spring, X. Qian, J. Cui and Z. Xu, *Sci. Rep.*, 2014, **4**, 5418.
19 L.-L. Li, K. Li, M.-Y. Li, L. Shi, Y.-H. Liu, H. Zhang, S.-L. Pan, N. Wang, Q. Zhou and X.-Q. Yu, *Anal. Chem.*, 2018, **90**, 5873-5878.
20 J.-y. Zhu, L.-f. Zhou, Y.-k. Li, S.-b. Chen, J.-w. Yan and L. Zhang, *Anal. Chim. Acta*, 2017, **961**, 112-118.
21 K. Rajasekhar, N. Narayanaswamy, N. A. Murugan, K. Viccaro, H.-G. Lee, K. Shah and T. Govindaraju, *Biosens. Bioelectron.*, 2017, **98**, 54-61.
22 Y. Li, K. Wang, K. Zhou, W. Guo, B. Dai, Y. Liang, J. Dai and M. Cui, *Chem. Commun.*, 2018, **54**, 8717-8720.
23 B. Guo, J. Jing, L. Nie, F. Xin, C. Gao, W. Yang and X. Zhang, *J. Mater. Chem. B*, 2018, **6**, 580-585.
24 L. Hou, P. Ning, Y. Feng, Y. Ding, L. Bai, L. Li, H. Yu and X. Meng, *Anal. Chem.*, 2018, **90**, 7122-7126.
25 J.-w. Yan, J.-y. Zhu, K.-x. Zhou, J.-s. Wang, H.-y. Tan, Z.-y. Xu, S.-b. Chen, Y.-t. Lu, M.-c. Cui and L. Zhang, *Chem. Commun.*, 2017, **53**, 9910-9913.
26 R. Guo, J. Yin, Y. Ma, G. Li, Q. Wang and W. Lin, *Sen. and Actuators B: Chem.l*, 2018, **271**, 321-328.
27 S. Humphries, *Proc. Natl. Acad. Sci. U. S. A.*, 2013, **110**, 14693-14698.
28 L. Wang, Y. Xiao, W. Tian and L. Deng, *J. Am. Chem. Soc.*, 2013, **135**, 2903-2906.